Dynamics of the Brainstem Action Selection System

José R. Donoso

Project dissertation for the MSc in Cognitive and Computational Neuroscience

Department of Psychology, University of Sheffield

Sheffield, S10 2TP, UK

2008

Abstract

The medial reticular formation (mRF) has been pointed as the most likely substrate for a brainstem action selection system. Additionally, a stochastic anatomical model has been proposed to assess potential configurations of action representation within the internal circuitry of the mRF. Under certain conditions, this anatomical model exhibits a rich oscillatory behaviour. The aim of this work is two-fold: First, to extend the exploration of the anatomical model by including oscillations and give a first step in testing hypothesis of action representation under the light of this emergent property. Second, to explore the model's structure-dynamics relationship in terms of its small-world-ness and its relevance for the oscillatory behaviour. It is proposed that assemblies of synchronised neurons are the dynamical functional units that codify an action (or subaction) or an overall behavioral state. It was found that different input levels applied on the same cluster bring out synchronised ensembles of neurons involving different areas of the network. No clear relation between dynamics and the structural property of small-world-ness was found throughout this work.

1 Introduction

1.1 Action representation on the mRF

The behavioral repertoire exhibited by decerebrated animals and neonates lacking fully operational basal ganglia suggests a brainstem based action selection system (Humphries, Gurney, & Prescott, 2007). Due to its unique input/output configuration and internal architecture, the medial reticular formation (mRF) has been proposed as a potential substrate for a brainstem action selection system (Humphries et al., 2007). Additionally, a combination of computational and robotic work has established considerable evidence for this hypothesis(Humphries, Gurney, & Prescott, 2005).

In the work carried out by (Humphries et al., 2007), a stochastic anatomical model was used to assess potential configurations of action representation within the internal circuitry of the mRF. Evidence of functional organisation based on common activity patterns leaded the authors to suggest a functional significance to the anatomical clustering exhibited by the mRF.

Three hypotheses of action representation were explored. Two of them considered a clustered representation where either (i) the output of each cluster could represent a complete action, or (ii) the clusters activate sub-actions, each one being a component of a coherent behaviour. The third alternative interpretation considered a non-local action representation by reinterpreting the 'modes' proposed by (Kilmer, McCulloch, & Blum, 1969) as simpler actions, and re-aiming the output of the model towards the activity projected to the spinal cord rather than to the ascending systems. Thus, the activity transmitted by an eventually-distributed group of projecting axons recruits the appropriate musculature for a given action (or sub-action). It is concluded that (ii) is the most likely scheme of action representation yet the coexistence of a clustered and parallel representations is left as an open possibility (Humphries et al., 2007).

Under certain conditions, the anatomical model exhibits a rich oscillatory behaviour. The aim of this work is to extend the exploration of the anatomical model (Humphries, Gurney, & Prescott, 2006) by including oscillations and give a first step in testing hypothesis of action representation under the light of this emergent property.

1.2 Oscillations and synchrony

Oscillations could be playing a major role in both ascending and descending systems of the mRF. If we consider the mRF projections to thalamus and cortex, oscillations could be of main importance in setting the global behavioral state of the animal (Kilmer et al., 1969) and in explaining the desynchronisation of the cortical electroencephalogram under stimulation of the mRF reported by (Moruzzi & Magoun, 1949). The interpretation can be pushed even further by considering the mRF as a 'higher order' CPG encoding a complex orchestration of patterns to drive lower level CPGs in order to express more complex behaviour. Moreover, this higher level CPG could be modulating the responsiveness of target neurons to upper motor neuron afferents by periodically elevating the membrane potentials of the target population providing time windows during which the target units are more likely to respond (Hutcheon & Yarom, 2000).

It has been claimed that synchronous activity of oscillating networks are the bridge between single-neuron activity and behaviour (Engel, Fries, & Singer, 2001). It is well known that single neurons are able to express complex dynamics such as resonance and oscillations at multiple frequencies (Hutcheon & Yarom, 2000) and it has also been suggested that information could be represented by the timing of their activity within the network (Buzsáki & Draguhn, 2004).

The main hypotheses of this work is that assemblies of synchronised neurons are the dynamical functional units that codify an action (or subaction) or an overall behavioral state. Consistent with this hypothesis, the degree of localisation of the neural representa-

tion will be assessed in terms of the degree of localisation of these neural assemblies. However, rather than directly attributing a role to synchronised assemblies either in assending or descending (motor) systems, the emphasis is put on the representational capacity of the system in terms of these neural ensembles.

1.3 Small-world-ness

One of the major findings of the work carried out by (Humphries et al., 2006) is that the mRF is most likely in a small-world regime. The characteristic properties found on this type of networks can be desirable in an oscillatory sensory-motor bridge such as the mRF; rapid synchronisation (Lago-Fernandez, Huerta, Corbacho, & Siguenza, 2000), consistent stabilisation (Li & Chen, 2003) and increased persistence of activity (Roxin, Riecke, & Solla, 2004) could facilitate the rapid establishment of stable and consistent (i.e. input specific) neural assemblies for a given set of sensory input patterns. The present work also explores the model's structure-dynamics relationship in terms of its small-world-ness.

1.4 Model and simulation parameters

Table 1: RF cluster model parameters

parameter	value	description
N_c	$N_c = 8$	Number of clusters in the model
n	$n = 50$	Number of neurons per cluster
ρ	$\rho = 0.8$	Proportion of projection neurons per cluster
ρ^-	$\rho^- = 0$	Proportion of projection neurons which are inhibitory
$P(c)$	$0 < P(c) \leq 1$	Inter-cluster collateral extension probability
$P(p \mid c)$	$0 < P(p \mid c) \leq 1$	Remote connection-given-collateral probability
$P(l)$	$0 < P(l) \leq 1$	Interneuron to local-neuron connection probability
ρ_s	$\rho_s = 1$	Proportion of projection neurons receiving sensory input
λ_s	$\lambda_s = 0.5$	Proportion of inter-neurons receiving sensory input
S_i	$0 \leq S_i \leq 1$	Input level at the ith cluster

The parameter values used for the stochastic model (Humphries et al., 2006) are

summarised on table 1. $P(c)$ is a distance dependent distribution defined according to $P(c_{ij}) = |i-j|^{-r}$, where c_{ij} is the event of a collateral extending from cluster i to cluster j $(i \neq j)$ and r is a free parameter that will be specified for each simulation. The number of clusters N_c is below the lower bound of the biological constrains estimated by (Humphries et al., 2006) and it was chosen for computational feasibility reasons. $P(l)$ and $P(p|c)$ are the main free parameters since they do not have supporting values in the literature (Humphries et al., 2007). The ρ value was set to the middle of the plausible range and λ_s was set to its maximum value due to the small proportion of interneurons set by the ρ value chosen. All the projection neurons and interneurons are excitatory and inhibitory, respectively. All the simulations were carried out during a time span of 3 seconds. The rest of the parameters were chosen according to the original study (Humphries et al., 2007). The activity of all the projection neurons during the time-span of the simulation is referred to as the 'output' of the model throughout this work. The terms 'unit' and 'neuron' are used indistinctively.

2 Structure and dynamics

2.1 Small-world analysis

In order to asses the 'small-world-ness' of a given instantiation of the model, its cluster coefficient C_s, characteristic path length L_s and corresponding values for an equivalent random network C_r and L_r were estimated. The 'small-world-ness' measure used is defined as $S = \gamma/\lambda$, where $\gamma = C_s/C_r$ and $\lambda = L_c/L_r$ (Humphries et al., 2006). After counting the number of edges n_e of a given instance of the model, the value of C_r was estimated according to the expected clustering coefficient of the equivalent directed random graph $C_r = n_e/(N(N-1))$ where N is the number of units (*i.e* edges) of the model(Fagiolo, 2007). L_r was estimated according to $L_r = 1 + \ln(n/z_1)/\ln(z_2/z_1)$ where z_1 and z_2

are the average numbers of first and second nearest neighbors from which a vertex can be reached, respectively (Newman, Strogatz, & Watts, 2001)(Boccaletti, Latora, Moreno, Chavez, & Hwang, 2006). C_s and L_s were estimated according to the definitions of (Watts & Strogatz, 1998)

For each $(P(l), P(p|c))$ pair taken from the parameters set $\Pi = \{[0.1, 1] \times [0.1, 1]\}$, a single instance of the stochastic model was generated and its small-world score was estimated. The parameters were taken from the set Π in steps of 0.1. The experiment was repeated for three different $P(c)$ distributions defined by values of r taken from $\{0.25, 0.75, 1.5\}$. For each value of r, a S-score surface was obtained. The three surfaces are depicted on figure 1.

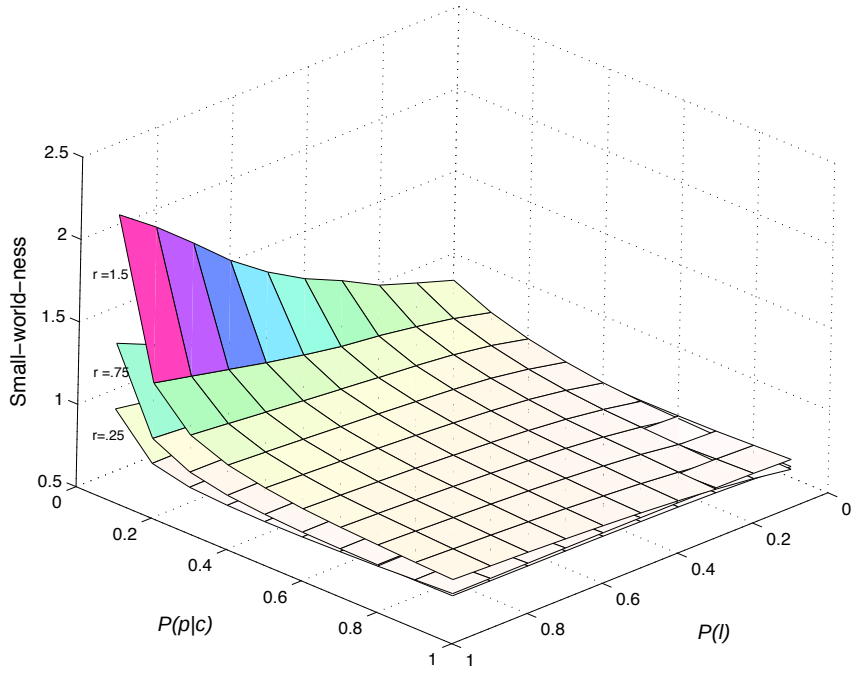

Figure 1: Small-world-ness for different values of $P(l)$ and $P(p|c)$. Different surfaces correspond to different values of $P(c)$ parametrised by r

For small networks like those generated in this study, $L_c \approx L_r$ so the S-score will be strongly governed by the γ factor(Montoya & Sole, 2002). In consequence, the parameters affecting the relative clustering coefficient C_s/C_r of the model instance will mainly affect

the S-score.

Since interneuron connections are confined within the cluster, higher values of P(l) will increase C_s. The higher the proportion of interneuron connections, the higher the chance of a given unit to contact two already linked units.

When $P(p|c)$ increases, the value of C_s decreases. Suppose a projection neuron c_p is contacting two projection units a_p and b_p. If a_p and b_p are both in the same cluster, the probability of both neurons being connected $P^c(a_p, b_p) = 0$ since two projection neurons within the same cluster cannot contact each other. In this case, the chance to increase C_s will be given by the probability of contacting interneuron-interneuron $(i - i)$ or interneuron-projection $(i - p)$ pairs that are already linked. Since the proportion of projection neurons is considerably higher than the proportion of interneurons, the most common case will be to contact unconnected pairs. The probability of finding $p - i$ or $i - i$ pairs are directly governed by $P(l)$. Therefore, the maximum clustering coefficient will occur at the maximum $P(l)$ and minimum $P(p|c)$. Since extra-cluster connections tend to degrade S, and the probability of establishing remote connections $\sim P(c)P(p|c)$, a higher value of r (more rapidly decaying P(c)) will improve C_s.

It is worth to mention that since the distance in the distance-dependent decaying of P(c) is defined in terms of cluster-number, the value of r must be adjusted according to the chosen N_c. A given value of r will describe a steeper decay in a network consisting of a larger number of clusters. Thus, the smaller the value of r used, the more P(c) resembles a uniform distribution. During the remaining of this section, the value of r will be set to 1.5 in order to encompass a wider span of S-scores within the $(P(l), P(p|c)$ space (see fig.1).

2.2 Global synchrony dependence on $P(l)$ and $P(p|c)$

The degree of synchrony within a set of unit outputs $\mathcal{S} \subset 1, 2, ..., n$ is defined according to

$$syn(\mathcal{S}) = \sigma\left(\frac{1}{|\mathcal{S}|}\sum_{i\in\mathcal{S}} x_i\right) \Big/ \frac{1}{|\mathcal{S}|}\sum_{i\in\mathcal{S}} \sigma(x_i) \tag{1}$$

where $|\mathcal{S}|$ is the cardinality of $\mathcal{S}$ and $\sigma(x)$ is given by (Lago-Fernandez et al., 2000).

$$\sigma^2(x) = \frac{1}{T_2 - T_1}\int_{T_1}^{T_2} \left[\langle x(t)\rangle_t - x(t)\right]^2 dt \tag{2}$$

which corresponds to the 'temporal variance'of the signal measured across the time span between T_1 and T_2.

In order to assess the dependence of the overall synchrony on the free parameters $P(l)$ and $P(p|c)$, several instances of the model were generated by taking $(P(l), P(p|c))$ pairs from the parameters set Π. For each instance of the model, a constant input level $S_4 = 0.1$ was applied on a single unit within the network ($\rho_s = 0.025$) and the synchrony measure defined on equation 1 was applied to the entire population output.

The above mentioned process was repeated 20 times, using different random seeds. This experiment was performed under four different conditions consisting in two different excitatory weight values (W) applied under under both balanced and unbalanced regimes. The surface plots depicted on figure 2 show the results of these experiments.

The abrupt increase in the overall synchrony of the network depicted along the $P(p|c)$ axis on figure 2.A suggests the existence a 'critical mass' of remote connections required to achieve full synchrony. Under the unbalanced regime, the negative effect of $P(l)$ is negligible due to the relative smaller amount of inhibitory connections.

Figure 2.B show the effect of decreasing W under the unbalanced regime. The remote connections have been weighted down and therefore the required 'critical mass' has increased proportionally. Again, the effect of $P(l)$ is negligible.

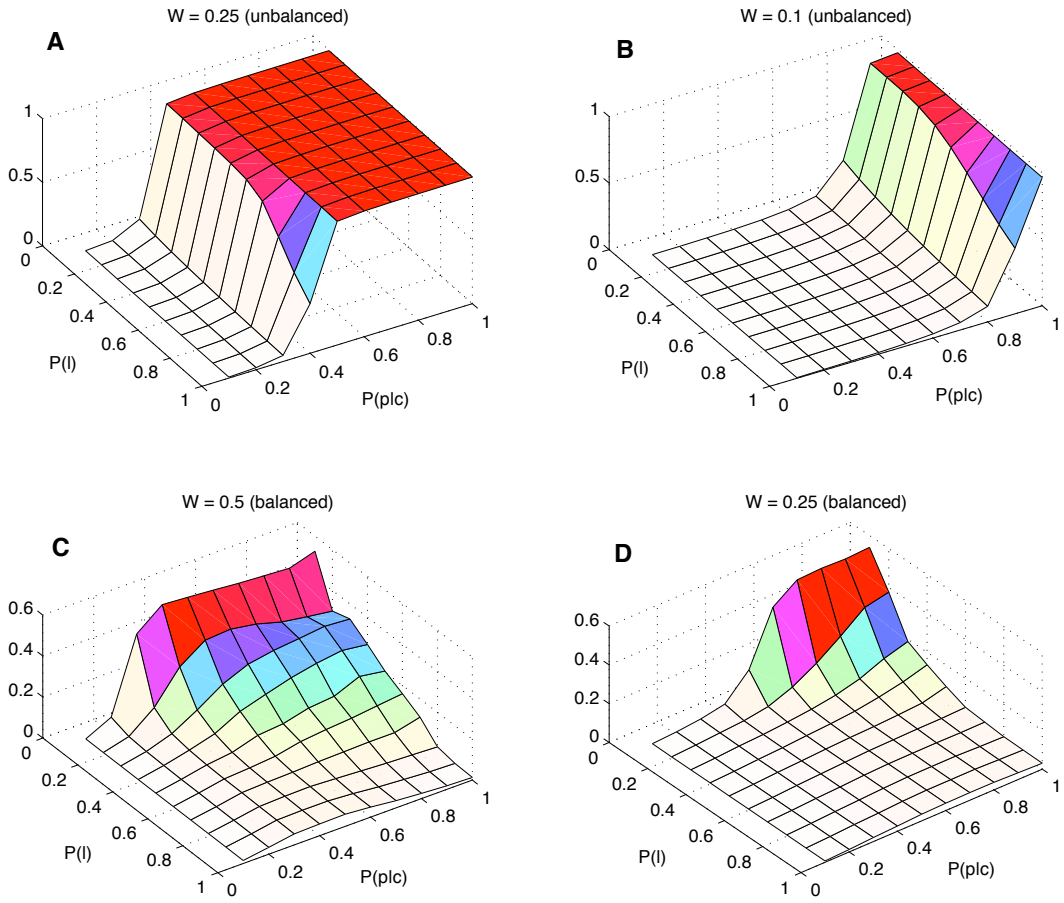

Figure 2: Overall synchrony dependence on $P(l)$ and $P(p|c)$ (Average over 20 experiments). **A-B.** Unbalanced network. Excitatory weights (W) set to 0.25 and 0.1, respectively. The decrease in W increases the critical value of $P(p|c)$ required for full synchrony. The effect of $P(l)$ is negligible due to the relative smaller amount of inhibitory connections. **C-D.** Balanced network. Excitatory weights (W) set to 0.5 and 0.25, respectively. Due to the balanced condition, the effect of P(l) becomes significant. *here*

Figures 2.C and 2.D Show the effect of balancing the weights. For values of $P(l) \approx 1$ many weak inhibitory connections are effectively counterbalancing the influence of remote afferent projecting neurons. As the value of $P(l)$ decreases, the number of i-p connections decreases. In spite their weights have been augmented proportionally, i-p connections cannot distribute uniformly along the entire population of projecting neurons within a given cluster permitting a foreign influence to propagate across the network. Thus, there's no

longer a 'critical mass' of remote connections and the steep change of synchrony becomes softer with increasing values of $P(l)$.

3 Input/Output Dynamics

3.1 Network coherence

Network coherence is of major importance since provides the environment for neural assemblies to emerge. Once coherence is achieved in a neural population, synchrony can be sustained even with very weak synaptic links as long as the frequency of the coupled oscillators remain similar(Buzsáki, Geisler, Henze, & Wang, 2004). It is therefore essential to rely on a consistent measure of network coherence before analysing the network response to cluster input.

One way to measure the degree of coherence of a temporal waveform is by fitting a gaussian to the highest peak of its power spectral density and calculating

$$\beta = \frac{H\omega}{\Delta\omega} \tag{3}$$

where H corresponds to the maximum value of the peak, ω its corresponding central frequency and $\Delta\omega$ its full width at half maximum(Gang, Ditzinger, Ning, & Haken, 1993).

For a perfectly coherent signal such as $cos(\omega t + \phi)$, $\Delta\omega \to 0$ and therefore $\beta \to \infty$. In practice, the use of finite sampling rates and constraints on the simulation output, set bounds on H and $\Delta\omega$.

I order to describe de global coherence of the network, a vector $\tilde{\beta}$ containing the values β_i for each ith output signal, is defined. A straightforward way to estimate the global coherence of the network would be to calculate the expected coherence of the population by averaging among all the elements of $\tilde{\beta}$ to obtain $\overline{\beta}$. However, the way β is defined in

addition to the limitation of its value for perfectly coherent signals makes $\overline{\beta}$ an unreliable estimator of global coherence.

The fact that β depends on both the amplitude and a bounded $\omega/\Delta\omega$ implies that low β values can result either from weak, perfectly coherent low-frequency signals ($H\omega \ll \Delta\omega$) and relatively stronger incoherent signals ($\Delta\omega \ll H\omega$). The inability to discriminate among these two cases creates several problems for $\overline{\beta}$ as a reliable estimator. This point will be illustrated by means of two examples.

e.g. **1** Suppose we have two simulation outcomes represented by two different sets $\mathcal{A}$ and $\mathcal{B}$ of fluctuating signals. Set $\mathcal{A}$ contains a few high amplitude, perfectly coherent signals embedded within a majority of highly incoherent ones yielding an average coherence $\overline{\beta_A}$. Set $\mathcal{B}$, contains only perfectly coherent but relatively weaker signals, each of which yields a $\beta_i = \overline{\beta_A}$. Both sets will exhibit the same $\overline{\beta}$ albeit set $\mathcal{B}$ should be clearly regarded as a more coherent configuration.

e.g. **2** Suppose that the two sets defined on *e.g.* 1 contain the same subset of perfectly coherent units but differ in the subset of non-coherent units. The non-coherent elements on set $\mathcal{A}$ consist of constant signals each of which as a $\beta_i \approx 0$. Set $\mathcal{B}$ contains incoherent fluctuating signals having the same β values as the non-coherent subset of $\mathcal{A}$. Again, both sets will be regarded as having the same global coherence.

In order to introduce a new coherence estimator. Consider the vectors $\tilde{\sigma^2}$ and $\tilde{\beta}$ describing the temporal variance and coherence of every signal in the set to be tested, respectively. By taking eq. (3) and noting that $\sigma^2(c) \propto H$ for a perfectly coherent signal $c(t)$, a simulation set consisting only of perfectly coherent signals of different amplitudes oscillating at the same frequency will exhibit a strongly linear dependence between the corresponding elements of the $\tilde{\sigma^2}$ and $\tilde{\beta}$ vectors.

If (σ_i, β_i) pairs taken from a set of perfectly coherent units oscillating at the same

frequency ω_s are scattered on a $\sigma - \beta$ plot, all the points corresponding to that set will lay on a straight line with a slope value depending on ω_s. Any unit oscillating at a different frequency or in an incoherent manner will lay away from the characteristic straight line. Moreover, if a given population is composed by different subsets oscillating at different frequencies, the points representing that population will lay in different lines according to the different slopes defined by the different subsets frequencies. Thus, the frequency variability within a set, as well as the number of incoherent oscillating signals will degrade the linear dependence between σ and β. Additionally, non-oscillating units will lay near the origin of the $\sigma - \beta$ space, leaving this linear dependence unaltered.

Consistently this, the correlation coefficient ζ between $\tilde{\sigma^2}$ and $\tilde{\beta}$ is proposed as a measure of network coherence, which is defined as

$$\zeta = \frac{cov(\tilde{\sigma^2}, \tilde{\beta})}{var(\tilde{\sigma^2})var(\tilde{\beta})} \tag{4}$$

and provides a measure of the linear dependence between $\tilde{\sigma^2}$ and $\tilde{\beta}$ indicating to which extent the units that are oscillating are doing it in a coherent manner.

3.2 Effect of cluster input level on network coherence

A single anatomical instantiation of the model was used to analyse the network output coherence response to different levels of input applied on different clusters. The free parameters were set to the values $r = 0.25$, $P(l) = 0.25$, $P(p|c) = 0.1$ and $W = 0.1$ under balanced regime in order to place the model within an oscillatory zone in the parameters space. For each cluster i in the model, the input was varied in steps of 0.1 along the range $S_i \in [0.11]$. The output-coherence-input characteristic $(\zeta - S_i)$ obtained for clusters $i = 1, 4, 6, 8$ are shown in3.

The most striking feature of the result, is the strong dependence of network coherence

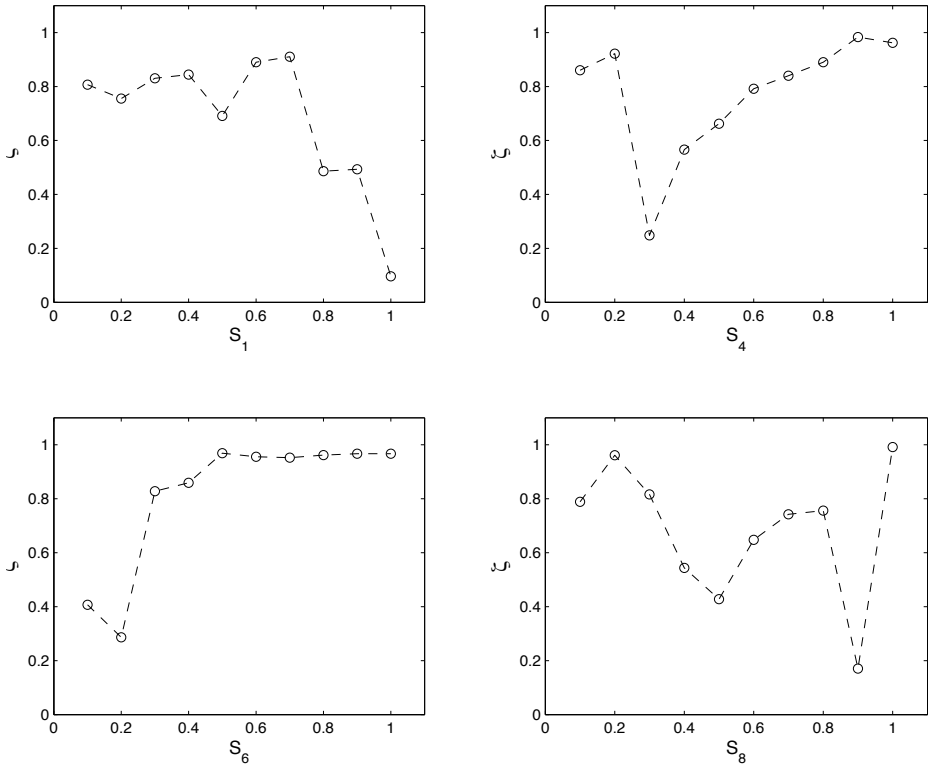

Figure 3: Network output coherence response to inputs applied on different clusters (S_1, S_4, S_6 and S_8). Network coherence responds in a characteristic way depending on which cluster the input is applied on.

on the input level. In a network with the same structural properties, global coherence values can span from 0.1 to > 0.9 solely due to the input level applied on a single cluster. Moreover, the dependence can follow different tendencies, either decreasing (as when S_1 is varied) or increasing (as when S_6 is varied) with input level or even present local minima and maxima (as when S_4 and S_8 are varied). The important point here is that output can sustain synchronous neural assemblies at different input levels depending on which cluster the input is applied on.

3.3 Effect of cluster input level on remote units synchrony

The emergence of neural assemblies was assessed by analysing the synchrony matrix M of the model output obtained from each experiment described in the previous section.

The synchrony matrix is defined according to $M_{ij} = M_{ji} = syn(\{i, j\})$, where $\{i, j\}$ is a pair of unit output indices and *syn* is the measure defined in equation (1). Thus, M is describing the dynamical connectivity of the network in a similar way a weighted adjacency matrix does with structural connectivity.

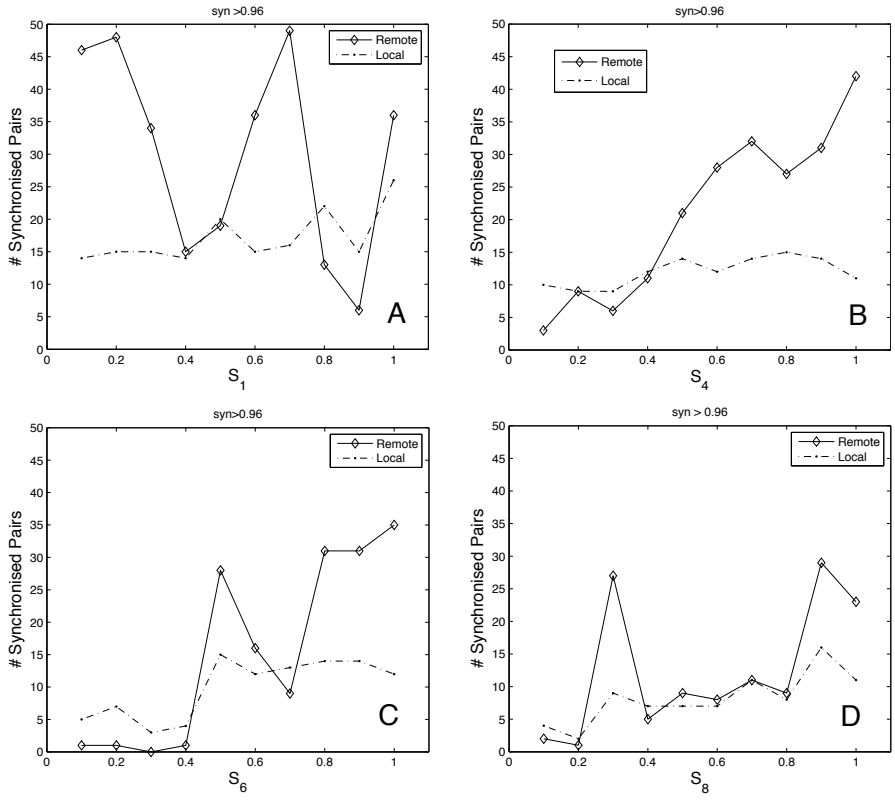

Figure 4: **A-D.** Number of remote and local synchronised units pairs emerging at different input levels. The synchronised pairs are all those ($\{i, j\}$) pairs with $syn(\{i, j\}) > 0.96$

One M was obtained from the entire output of the model for each S_i value. From each M, the number of local and remote synchronised pairs were extracted, where a synchronised pair is defined as $\{i, j\} : sync(\{i, j\}) > 0.96$, local pairs are defined as

those contained within the same cluster and remote pairs as those contained in different clusters. The threshold value of synchrony (0.96) corresponds to the value obtained from two sinusoids de-phased by 30^o. Figure 4, shows the counts of synchronised local and remote pairs for a given input level applied at clusters $1, 4, 6$ and 8.

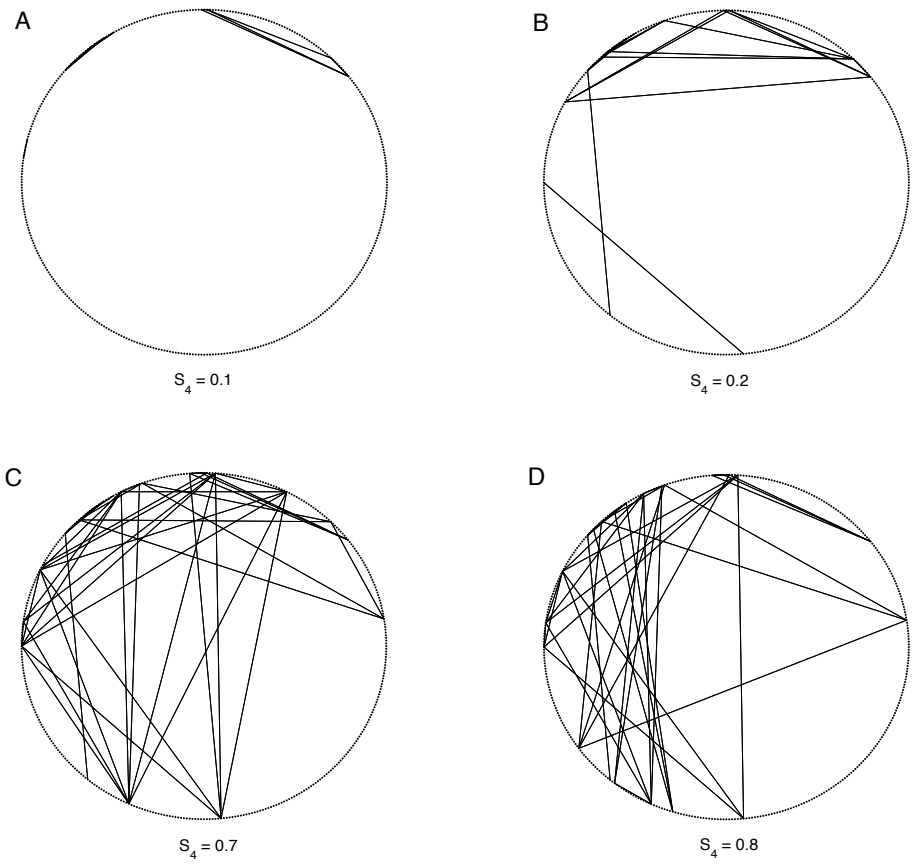

Figure 5: **A-D.** Graphs showing the different ensembles emerging at different input levels applied on cluster 4 (S_4). Units pairs with $syn > 0.96$ are joined by a straight line.

From this particular results, it can be seen that the number of synchronised pairs are dominated by remote clusters links. Comparatively, the number of local pairs formed do not vary considerably with input level. The fact that the number of remote pairs strongly varies with input level suggests a distributed representation in terms of synchrony. In order to assess this possibility graphs, were constructed from binary adjacency matrices

taken from M by assigning a 1 for all $M_{ij} > 0.96$ and a 0 for all $M_{ij} \leq 0.96$. In figure 5 the graphs corresponding to four values of S_4 are shown. The graphs shown were taken at input levels were the network exhibited high coherence. It is clear on this case the emergence of different neural ensembles for different input values.

Careful examination of figure 5 evidences how relatively close values of input level applied on the same cluster bring out ensembles of neurons involving different areas of the network. The transition from $S_4 = 0.1$ to $S_4 = 0.2$ (Fig. 5.A-B) involves the recruitment of a considerable number of remote units. The transition from $S_4 = 0.7$ to $S_4 = 0.8$ (Fig. 5.C-D) does not involve a considerable recruitment of additional units (see fig. 4.B) but clearly show how different set of neurons become synchronised.

4 Conclusions

The fact that the model is able to express synchronised activity among different populations of neurons depending on the input level applied to a particular cluster has major implications for both the explanatory power of the model and its encoding capacity.

If neurons within a given cluster are contacting a specific subset of passing fibers, the input level of a cluster in the model can be interpreted as representing the correlation among the activities of those fibers. Under the light of the findings described on the last section, the correlated activation of a particular set of fibers can trigger the recruitment of different oscillating neural assemblies that, in turn could activate unique sets of downstream population contacted by both the ascending and descending systems of the mRF.

If we consider the mRF projections to the thalamus and cortex, these ensembles of oscillators are in a good position to explain the desynchronisation of the cortical electroencephalogram under stimulation of the mRF reported by (Moruzzi & Magoun, 1949).

There is evidence that out of phase rhythmic activity can selectively suppress oscillations in the target networks, an example of this is the suppression of gamma-frequency rhythm in the hippocampus by the dentate gyrus input (Csicsvari, Jamieson, Wise, & Buzsaki, 2003). This is also consistent with the interpretation that the mRF acts as a 'mode selector' which sets the global behavioral state of the animal (Kilmer et al., 1969).

It is clear from the results on local v/s remote synchronised pairs, that neural assemblies are more likely to be composed by units from different clusters. If an hypothesis of action representation in terms of synchronised oscillatory behavior is to be made, the evidence found in this work points towards a distributed one.

The inter-cluster nature of neural assemblies allows the system to encode a huge variety of output behaviours that could be further multiplied by the available modes of oscillation in the network. Further exploration of the model should assess its capacity to oscillate coherently at different frequencies simultaneously.

Since this is not a spiking model, care must be taken when interpreting oscillations and synchrony. Usually, the oscillatory behavior is studied as an emergent property of large models composed by spiking units (Lago-Fernandez et al., 2000), and synchrony is studied in terms of spike co-occurrence among their outputs (Masuda & Aihara, 2004). However, in models composed of leaky integrators (LIs), where oscillations emerge at the unit level, synchrony does not constitute a reliable measure of spiking co-occurrence. While it's true that synchronised oscillatory LIs are somehow representing two neurons that are more likely to co-fire, it is also true that two synchronised LI's could be also representing two silent neurons whose respective membrane potentials are oscillating under subthreshold regime. Therefore, if the oscillatory behavior of the model is to be seriously considered, the units should be updated to a spiking neuron model.

No clear relation between dynamics and the structural property of small-world-ness was found throughout this work.

References

Boccaletti, S., Latora, V., Moreno, Y., Chavez, M., & Hwang, D.-U. (2006). Complex networks: Structure and function. *Physics Reports*, *424*, 175–308.

Buzsáki, G., & Draguhn, A. (2004, June). Neuronal oscillations in cortical networks. *Science*, *304*(5679), 1926–1929.

Buzsáki, G., Geisler, C., Henze, D. A., & Wang, X. J. (2004, April). Interneuron diversity series: Circuit complexity and axon wiring economy of cortical interneurons. *Trends Neurosci*, *27*(4), 186–193. Available from `http://dx.doi.org/10.1016/j.tins.2004.02.007`

Csicsvari, J., Jamieson, B., Wise, K. D., & Buzsaki, G. (2003, January). Mechanisms of gamma oscillations in the hippocampus of the behaving rat. *Neuron*, *37*(2), 311–322. Available from `http://dx.doi.org/10.1016/S0896-6273(02)01169-8`

Engel, A. K., Fries, P., & Singer, W. (2001, October). Dynamic predictions: oscillations and synchrony in top-down processing. *Nat Rev Neurosci*, *2*(10), 704–716. Available from `http://dx.doi.org/10.1038/35094565`

Fagiolo, G. (2007). Clustering in complex directed networks. *Phys Rev E*, *76*, 026107.

Gang, H., Ditzinger, T., Ning, C. Z., & Haken, H. (1993, Aug). Stochastic resonance without external periodic force. *Phys. Rev. Lett.*, *71*(6), 807–810.

Humphries, M. D., Gurney, K., & Prescott, T. J. (2005). Is there an integrative center in the vertebrate brainstem? a robotic evaluation of a model of the reticular formation viewed as an action selection device. *Adapt. Behav.*, *13*, 97–113.

Humphries, M. D., Gurney, K., & Prescott, T. J. (2006). The brainstem reticular formation is a small-world, not scale-free, network. *Proc. Roy. Soc. B.*, *273*, 503–511. (doi:10.1098/rspb.2005.3354)

Humphries, M. D., Gurney, K., & Prescott, T. J. (2007). Is there a brainstem substrate for action selection? *Phil Trans R Soc B*, *362*, 1627–1639.

Hutcheon, B., & Yarom, Y. (2000, May). Resonance, oscillation and the intrinsic frequency preferences of neurons. *Trends Neurosci*, *23*(5), 216–222. Available from http://view.ncbi.nlm.nih.gov/pubmed/10782127

Kilmer, W. L., McCulloch, W. S., & Blum, J. (1969). A model of the vertebrate central command system. *Int. J. Man Mach. Stud.*, *1*, 279–309.

Lago-Fernandez, L. F., Huerta, R., Corbacho, F., & Siguenza, J. A. (2000). Fast response and temporal coherent oscillations in small-world networks. *Physical Review Letters*, *84*, 2758–2761.

Li, C., & Chen, G. (2003). Stability of a neural network model with small-world connections. *Phys Rev E*, *68*, 052901.

Masuda, N., & Aihara, K. (2004). Global and local synchrony of coupled neurons in small-world networks. *Biol Cybern*, *90*, 302–309.

Montoya, J. M., & Sole, R. V. (2002, February). Small world patterns in food webs. *Journal of Theoretical Biology*, *214*(3), 405–412. Available from http://dx.doi.org/10.1006/jtbi.2001.2460

Moruzzi, G., & Magoun, H. W. (1949). Brain stem reticular formation and activation of the EEG. *Electroenceph. clin. Neurophysiol.*, 455–473.

Newman, M. E., Strogatz, S. H., & Watts, D. J. (2001). Random graphs with arbitrary degree distributions and their applications. *Phys Rev E*, *64*, 026118.

Roxin, A., Riecke, H., & Solla, S. A. (2004, May). Self-sustained activity in a small-world network of excitable neurons. *Physical Review Letters*, *92*(19), 198101+. Available from http://dx.doi.org/10.1103/PhysRevLett.92.198101

Watts, D. J., & Strogatz, S. H. (1998, June). Collective dynamics of 'small-world' networks. *Nature*, *393*(6684), 440–442. Available from http://dx.doi.org/10.1038/30918